International Journal of Fluid Power 4 (2003) No. 1 pp. 31-39

MODELLING OF ORIFICE FLOW RATE AT VERY SMALL OPENINGS

Duqiang Wu, Richard Burton, Greg Schoenau and Doug Bitner

Department of Mechanical Engineering, University of Saskatchewan, 57 Campus Drive, Saskatoon, Saskatchewan, Canada, S7N 5A9
duw612@mail.usask.ca

Abstract

Modelling hydraulic control systems that contain flow modulation valves is highly influenced by the accuracy of the equation describing flow through an orifice. Classically, the basic orifice flow equation is expressed as the product of cross-sectional area, the square root of the pressure drop across the orifice and a "flow discharge coefficient", which is often assumed constant. However, at small Reynolds numbers (such the case of valve pilot stage orifices), the discharge coefficient of the flow equation is not constant. Further, the relationship between the flow cross-sectional area and the orifice opening are extremely complex due to clearances, chamfers, and other factors as a result of machining limitations. In this work, a novel modification to the flow cross-sectional area is introduced and the resulting closed form of the flow equation is presented. As a secondary benefit, an analytical form of the orifice flow gain and flow pressure coefficient can be obtained. This closed form equation greatly facilitates the transient and steady state analysis of low flow regions at small or null point operating regions of spool valve.

Keywords: pilot valve, flow control, orifice, flow rate equation, discharge coefficient, Reynolds number

1 Introduction

In many fluid power applications, spool valves are used to modulate flow to a load. This flow can be quite large and demonstrate turbulent behavior. Under these conditions, the discharge coefficient is known to be constant and independent of the Reynolds number. However in other applications, the flow through the valve can be very small and show a strong dependency on the Reynolds number. Such applications of low flow rate are often found in pilot valves of two stage valves or in compensators of pumps and motors. For these kinds of applications, it is very difficult to model the flow rate because the flow cross-sectional area around the null position often cannot be exactly defined or because the flow may not be turbulent. Due to these difficulties, other means such as experimental techniques are often used to model the flow (Bitner, 1986). Chaimowitsch (1967) developed a flow model for a rectangular orifice as a function of pressure drop and geometry parameters (clearance, chamfer angle, openings, the maximum lap, etc.). The model is difficult to use due to its extremely complex form. Therefore, an accurate and relatively simple analytical expression of flow is absolutely essential in order to develop a complete dynamic model of any hydraulic control system.

This manuscript was received on 11 October 2002 and was accepted after revision for publication on 18 December 2002

Consider the classical square-type orifice flow equation. As derived from Bernoulli's equation, flow is proportional to the product of the orifice width, the orifice opening, the square root of the pressure drop and a flow coefficient which is defined as the discharge coefficient. The equation is derived by assuming the fluid is inviscid, incompressible, one dimensional and turbulent. Thus,

$$Q = C_{\mathrm{d}} w x \sqrt{\frac{2}{\rho}\Delta P} \tag{1}$$

In most applications, for large Reynolds numbers, C_{d}, is modelled as being constant. Merritt (1967) suggests that the application of the general turbulent flow equation (Eq. 1) can also be extended to the case of laminar flow. However, the discharge coefficient, C_{d}, is now a function of the Reynolds number, as well as the orifice geometry. C_{d} is usually determined experimentally and presented graphically. However, in Wu (2002), a closed form model of the discharge coefficient was developed for different types of orifice geometries. This closed form expression for a square-type orifice is

$$Q = C_{\mathrm{d}\infty}\left(1 + a\mathrm{e}^{-\frac{\delta_1}{C_{\mathrm{d}\infty}}\sqrt{Re}} + b\mathrm{e}^{-\frac{\delta_2}{C_{\mathrm{d}\infty}}\sqrt{Re}}\right) w x \sqrt{\frac{2}{\rho}\Delta P} \tag{2}$$

The advantage of Eq. 2 is that it is possible to differentiate the flow rate to obtain flow gain, $K_{\mathrm{q}} = \partial Q/\partial x$,

© 2003 TuTech

and flow pressure coefficient, $K_c = \partial Q/\partial P$, for use in transient and stability studies. Palmberg (1985) and Wu (2002) showed that stability in a load sensing system is influenced by the parameters K_q and K_c, which are important factors in determining the overall pump gain and dynamic behavior of the pump. Others (Krus, 1988; Lantto, 1990, 1991; Peterson, 1996) have also shown that stability is influenced by overall pump gain.

At small orifice openings around the null point, Eq. 1 and 2 are often invalid. This is because the actual flow cross-sectional area, *A*, is not defined due to clearances, chamfers and other factors which result from machining limitations. Figure 1 shows a comparative plot of an ideal flow rate based on Eq. 1 or 2 and a measured flow rate about the null point. It is evident that a significant error between the measured and ideal flow does occur at the null position. Further, for the curve illustrated in this figure, the flow gain, which from Eq. 1 or 2 should be constant for $x > 0$, is not constant in actual practice. For $x < 0$, the theoretical flow gain is zero, but in actual practice is still a positive, finite value. Thus, it is necessary to develop an empirical expression that will approximate the typical flow rate for $-\alpha < x < \alpha$. To do this, it is necessary to accurately model the orifice area in some empirical function.

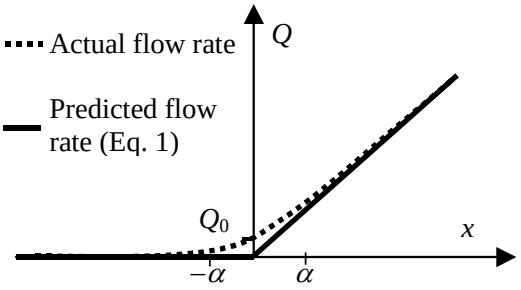

Fig.1: *Comparison of measured and ideal flow rates for a typical pilot valve*

The objective of this paper is to present an empirically modified closed form of the flow cross-sectional area, *A*, which would replace *wx* in Eq. 2 and which could be used to accurately model the flow equation in the null region. This empirical form will allow the flow orifice equation to be valid at small openings (positive and negative), as well as large spool displacements, *x*.

2 Modelling of the Cross-sectional Area of an Orifice

The model of flow cross-sectional area of an orifice, $A(x)$, is highly dependent on the geometry of the orifice (often defined as "square", "crescent", "short slot tube" etc). This study assumes that the orifice is rectangular, which is the most common types. Other types can be modelled in a similar fashion. Figure 2 illustrates a typical rectangular orifice in a spool valve. At the null position, the existence of clearances result in null position flow; thus at $x = 0$, an equivalent flow cross-sectional area must be defined. In the absence of any chamfers on the land, the cross-sectional area is

$$A = \frac{\left(D_2^2 - D_1^2\right)\pi}{4} \tag{3}$$

where D_1 and D_2 are the diameters of the spool and sleeve respectively. For convenience, the cross-sectional area, *A*, can be alternatively expressed in terms of the clearance between the spool and sleeve, *c*, and the average diameter, *D*. In order to do this, consider the relationships as follows (see Fig. 2)

$$D_1 = D - c \tag{4}$$

$$D_2 = D + c \tag{5}$$

Substituting Eq. 4 and 5 into Eq. 3 gives

$$A = \pi \cdot D\, c = w\, c \tag{6}$$

where *w* is defined as the width of the square orifice at the null position and is equal to the average of the perimeters of the spool and sleeve. *c* is defined as the height of the square orifice. It is noted that Eq. 6 has the same form as the cross-sectional area term, *wx*, in Eq. 2. However, at the null position, *A* would be zero but in practical applications, the existence of spool clearances means this is not valid.

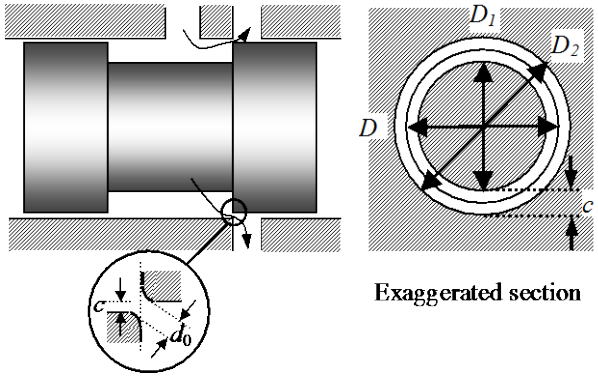

Fig. 2: *Flow cross sectional areas of a rectangular orifice*

The flow cross-sectional area due to clearances is even larger than *wc* at the null position due to chamfers. The height of the rectangular orifice is, in fact, d_0, instead of *c* (see Fig. 3b). Assuming that the chamfer angle radius is *r*. The height of the orifice, d_0, can now be expressed as

$$d_0 = \sqrt{(2r + c)^2 + 4r^2} - 2r \tag{7}$$

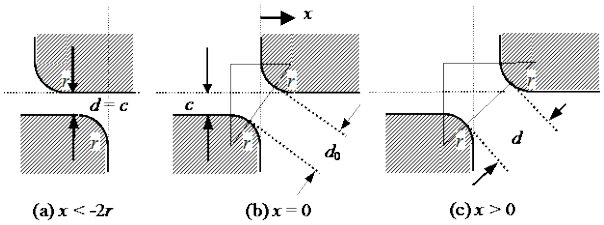

Fig. 3*: The enlarged scenario of the spool and sleeve chamfers*

When the spool is not at null position (see Fig. 3a and 3c), the height, d_0, becomes

$$d(x)=\begin{cases}\sqrt{(2r+c)^2+(2r+x)^2}-2r & x>-2r\\ c & x<-2r\end{cases} \quad (8)$$

Therefore, the cross-sectional area becomes

$$A(x)=wd(x)$$
$$=\begin{cases}w\left(\sqrt{(2r+c)^2+(2r+x)^2}-2r\right) & x>-2r\\ wd_0 & x=0\\ wc & x<-2r\end{cases} \quad (9)$$

However, it is not convenient to use Eq. 9 in Eq. 2, because:

- Equation 9 is valid only for a known quarter circular chamfer. Whereas the actual land chamfer geometry would not be known,
- Equation 9 includes two parameters, r and c which would be very difficult to measure and
- Equation 9 is complex and piecewise.

When the spool displacement, x, is less than $-2r$, the orifice cross-sectional area in Eq. 9 becomes constant and subsequently for a constant pressure drop, the flow rate would become a constant (Eq. 2). However in reality, the flow rate is not constant but decreases as the lap increases (Fig. 3a). This is because the orifice now becomes a short slot tube and hence the coefficients (i.e., $C_{d\infty}$, a, b, δ_1 and δ_2) in the discharge coefficient model for a typical square orifice become invalid. For the above reasons, it is necessary to consider developing an empirical flow area model that reflects the behaviors of Eq. 9 for $x > -2r$ and approximates the flow of short slot tube orifice for $x < -2r$ in the same flow rate model.

Any empirical model requires experimentally generated data. Considering Fig. 2, if the spool is fixed at a certain position, the pressure drop across the orifice, ΔP, and the flow rate through the orifice, Q, are readily measured. The flow cross-sectional area, A, can be estimated by Eq. 1 (accounting for the changing C_d as in Wu (2002)). As in any experimental procedure, measurement error will have an effect on the estimated value of A. This results in the vertical scatter in the data in Fig. 4. Any error in estimating C_d will also contribute to the scatter.

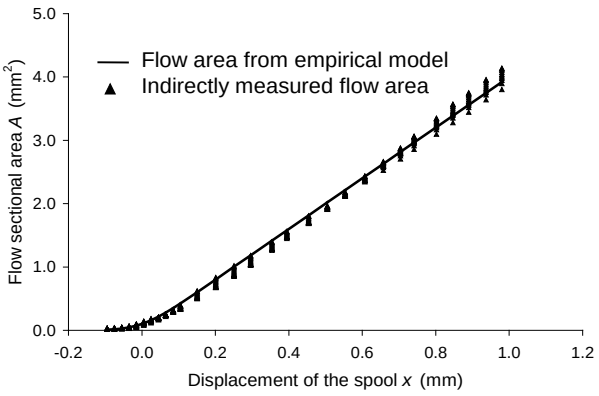

Fig. 4: *The measurement and modelling of the orifice flow cross sectional area*

The objective is to find an empirical relationship between the flow cross-sectional area, A, and the spool displacement, x, which will best fit the experimental results. There are many functions that can be used to fit the data, including an n^{th} order polynomial. However, the function that would be most desirable is one that would satisfy the following constraints:

- The functional form should be as simple as possible.
- The function should not include more than two parameters (one would be ideal) in addition to the orifice width, w ($w = D\pi$). These parameters should have some physical significance.
- The fit should be acceptable at large spool displacements as well as in the region about the null position.

In this study, an empirical model which satisfies the above criteria is proposed as

$$A(x)=\frac{wx}{1-e^{-\frac{x}{d_0}}} \quad (10)$$

where w is the width of the square type orifice and d_0 is a parameter which can be related to the equivalent orifice height at the null position (refer to Fig.3 b). The clearances and chamfers influence the model though the term, $\frac{1}{1-e^{-\frac{x}{d_0}}}$. Because it is difficult to obtain d_0 analytically from Eq. 7, d_0 is experimentally determined from

$$d_0=\frac{A|_{x=0}}{w} \quad (11)$$

where

$$A|_{x=0}=\frac{1}{N}\sum_{i=1}^{N}\frac{Q_i}{C_d\sqrt{\frac{2}{\rho}\Delta P_i}} \quad (12)$$

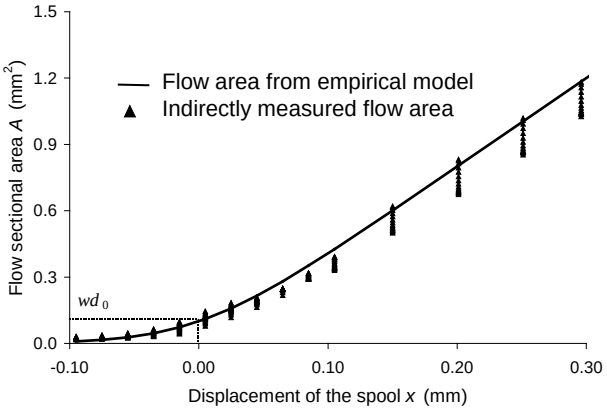

Fig. 5*:* *The measurement and modeling of the orifice flow cross sectional area about the null position*

In Eq. 12, N is the number of measurements at different pressure drops, ΔP_i. C_d is determined by Wu´s (2002) model. For non-rectangular orifice, w varies with position. In this case, Eq. 10 is used with a small non-zero valve displacement to generate another equation in w and d_0 from which an effective valve width can be cal-

culated. In Fig. 4, Eq. 10 is plotted as the solid line for the valve used in this study. Figure 5 shows more closely the information in Fig. 4 about the null position.

The model must satisfy the following boundary conditions:

- When x is a large negative number (large lapped amounts), $A \to 0$ and $\partial A/\partial x = 0$.
- When $x = 0$, $A = wd_0$.
- When x is a large positive number (large openings), $A \to wx$.

From Fig. 4 and 5, it is apparent that the first and third boundary conditions are satisfied. When $x = 0$, Eq. 2 tends to 0/0. Applying L′Hopital rule to Eq. 10 gives

$$A\Big|_{x=0} = \lim_{x\to 0} A(x) = \frac{\left.\dfrac{d(wx)}{dx}\right|_{x=0}}{\left.\dfrac{d}{dx}\left(1-e^{-\frac{x}{d_0}}\right)\right|_{x=0}} = wd_0 \qquad (13)$$

Thus, the second condition is satisfied.

Equation 13 and Fig. 5 indicate that, although the null position is a singular point, Eq. 10 is continuous. As a consequence, the flow rate equation (Eq. 2) is also continuous.

3 Analytical Model of the Flow Gain and Flow Pressure Coefficient

Using the modified form of Eq. 10 for the flow cross-sectional area, the flow through the orifice becomes

$$Q = C_{d\infty}\left(1 + a\mathrm{e}^{-\frac{\delta_1}{C_{d\infty}}\sqrt{Re}} + b\mathrm{e}^{-\frac{\delta_2}{C_{d\infty}}\sqrt{Re}}\right)\frac{wx}{1-\mathrm{e}^{-X}}\sqrt{\frac{2}{\rho}\Delta P} \qquad (14)$$

where $X = x/d_0$. X is a dimensionless variable.

The flow gain and the flow pressure coefficient can be obtained by differentiating Eq. 14 with respect to the opening, x, and pressure drop, ΔP. As developed in Appendix A, the closed forms for K_q and K_c become

$$K_q = \frac{\partial Q}{\partial x} = \frac{C_d w}{1-\varepsilon}\frac{\left(1-(1+X)\cdot\mathrm{e}^{-X}\right)}{\left(1-\mathrm{e}^{-X}\right)^2}\sqrt{\frac{2}{\rho}\Delta P} \qquad (15)$$

and

$$K_c = \frac{\partial Q}{\partial \Delta P} = \frac{C_d w x}{(1-\varepsilon)\left(1-\mathrm{e}^{-X}\right)\sqrt{2\rho\Delta P}} \qquad (16)$$

where

$$\varepsilon = \frac{\left(-a\delta_1 e^{-\frac{\delta_1}{C_{d\infty}}\sqrt{Re}} - b\delta_2 e^{-\frac{\delta_2}{C_{d\infty}}\sqrt{Re}}\right)\sqrt{Re}}{2C_d} \qquad (17)$$

It is apparent that the "modification" quantity, ε, is also a function of the Reynolds number (Eq. 17). It can be shown that at $Re = 0$, $\varepsilon = 0.5$ (Note: as $Re \to 0$, $C_d \to 0$ as well). For a typical sharp-edged orifice, ε is plotted in Fig. 6 and varies from 0.5 at very low Reynolds numbers to zero at large Reynolds numbers. It should be noted here that at $x = 0$, Eq. A12, A13 and A14 (see Appendix A) should be used rather than Eq. 15, 16 and 17. A simple "IF" statement can be used to facilitate this in a dynamic simulation.

Equation 14, 15 and 16 are the general forms of the flow rate through a square orifice, the flow gain and flow pressure coefficient respectively, which can be applied to cases of laminar flow, turbulent flow, as well as the transition from laminar to turbulent flow. For both laminar flow and turbulent flow, Eq. 15 and 16 can be simplified as follows.

As the orifice opening, x, and/or the pressure drop, ΔP, increase, the Reynolds number increases. C_d and ε converges to $C_{d\infty}$ and 0 respectively. If $x >> d_0$ (i.e., $X >> 1$), the term, $\dfrac{\left(1-(1+X)\cdot\mathrm{e}^{-X}\right)}{\left(1-e^{-X}\right)^2}$, also converges to 1. As a result, the flow gain becomes the well-known form of

$$K_q\Big|_{\text{turbulent}} = C_{d\infty} w\sqrt{\frac{2}{\rho}\Delta P} \qquad (18)$$

and the flow pressure coefficient becomes the familiar expression

$$K_c\Big|_{\text{turbulent}} = \frac{C_{d\infty} w x}{\sqrt{2\rho\Delta P}} \qquad (19)$$

It would appear from Eq. 19 that K_c could become infinite when $\Delta P = 0$. This is not true as K_c is always a finite value. When ΔP approaches zero, the flow rate is very small and the flow becomes laminar. Therefore, Eq. 19 is really not applicable. In this situation, the Reynolds number is very small and thus Eq. 16 should be used under the limit, C_d approaches zero. Thus, as shown in Appendix B, the closed forms of the flow gain and the flow pressure coefficient under laminar flow conditions are

$$K_a\Big|_{\text{laminar}} = \frac{8\delta^2 wx\Delta P}{\mu}\cdot\frac{1-(1+X)\cdot\mathrm{e}^{-X}}{\left(1-\mathrm{e}^{-X}\right)^3} \qquad (20)$$

$$K_c\Big|_{\text{laminar}} = \frac{4wx^2\delta^2}{\mu\left(1-\mathrm{e}^{-\frac{x}{d_0}}\right)^2} \qquad (21)$$

where δ is the laminar discharge coefficient, as defined in Wu (2002). Under these conditions, it can be observed that the flow pressure coefficient, K_c, is independent of the pressure drop, ΔP, across the orifice under the laminar flow conditions.

When $x = 0$, the flow rate (leakage) is through the clearances and hence is small. The flow is usually laminar. Therefore, Eq. 20 and 21 are applicable. The flow gain and the flow pressure coefficient at $x = 0$ thus become

$$K_{q0} = \left.\frac{\partial Q}{\partial x}\right|_{x=0} = \frac{4\delta^2 w d_0 \Delta P}{\mu} \tag{22}$$

$$K_{c0} = \left.\frac{\partial Q}{\partial \Delta P}\right|_{x=0} = \frac{4\delta^2 w d_0^2}{\mu} \tag{23}$$

Equation 14, 15 and 16 can also be extended to the case of non-rectangular orifices. The general forms of the flow rate, the flow gain and the flow pressure coefficient for any type orifice can be expressed by

$$Q = C_d \frac{A(x)}{1-e^{-X}} \sqrt{\frac{2}{\rho}\Delta P} \tag{24}$$

$$K_q = \frac{C_d w}{1-\varepsilon} \frac{\left(1-(1+X)\cdot e^{-X}\right)}{\left(1-e^{-X}\right)^2} \sqrt{\frac{2}{\rho}\Delta P} \tag{25}$$

$$K_c = \frac{C_d A(x)}{(1-\varepsilon)\left(1-e^{-X}\right)\sqrt{2\rho\Delta P}} \tag{26}$$

where $A(x)$ represents the ideal area as a function of the orifice opening (without considering clearances and chamfers). C_d employs Wu´s (2002) model. X and w represent the area ratio of the ideal area function, $A(x)$, and the practical leakage area, A_0, at the null position, and the equivalent orifice width respectively, i.e.,

$$C_d = C_{d\infty}\left(1 + a e^{-\frac{\delta_1}{C_{d\infty}}\sqrt{Re}} + b e^{-\frac{\delta_2}{C_{d\infty}}\sqrt{Re}}\right) \tag{27}$$

$$X = \frac{A(x)}{A_0} \tag{28}$$

$$w = \frac{dA(x)}{dx} \tag{29}$$

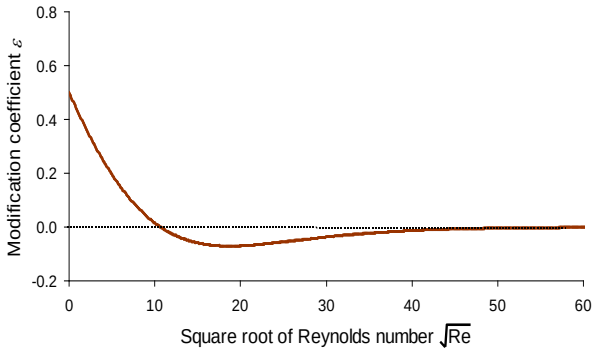

Fig. 6: *The modification of the discharge coefficient for orifice flow gain and flow pressure coefficient*

4 A Comparison of the Analytical and Experimental Results

The orifice flow rate models expressed by Eq. 14, 15, and 16 can be verified experimentally. A pilot valve was used in the experimental verification (Fig. 7). With the orifice opening, x, fixed, the flow rate, Q, and the pressure drop, $\Delta P = P_u - P_d$, were measured. Experimental results of flow through a pilot valve with a crescent orifice were obtained and illustrated using the function, $Q(x)$ at a specific pressure drop, ΔP, and the function, $Q(\Delta P)$ at a specific opening, x.

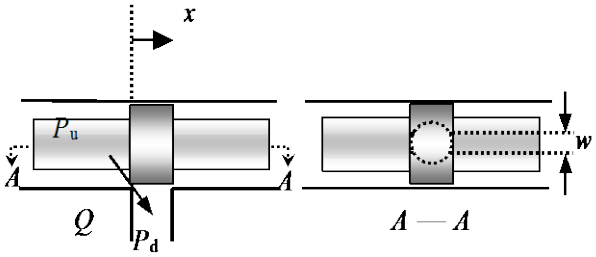

Fig. 7: *A simple spool orifice*

In order to calculate the flow rate using the empirical model provided in this study, parameters for the cross-sectional area model, w and d_0, and parameters for the discharge coefficients model, $C_{d\infty}$, a, b, δ_1 and δ_2, must be known. Although the cross-sectional area is a crescent type (see Fig. 7), experimental results indicate that, within small orifice openings, such as less than 1 mm (in this study), the orifice could be approximated as a rectangular type. For the pilot valve used in this study, the identified model parameters, w and d_0, are listed in Table 1. Wu´s (2002) research indicated that model parameters of the discharge coefficient, $C_{d\infty}$, a, b, δ_1 and δ_2, were highly dependent on the orifice geometry, such as "sharp-edged", "short slot tube", or "needle valve" types. In this study, the pilot valve used was a sharp-edged type and the model parameters are also given in Table 1.

Table 1: Model parameters

d_0(mm)	w(mm)	$C_{d\infty}$	a	δ_1	b	δ_2
0.025	4	0.63	-0.99	0.20	-0.01	3.7

Figure 8 shows a comparison of the flow rate using Eq. 14 and the experimental results for orifice flow rates at small openings ($x > 0$) and small lapped amounts ($x < 0$) for a pressure drop of 5 MPa. All the experimental data is contained in the region between the two dashed lines. Although the empirically calculated flow is not a perfect fit to the experimental results, it is far superior to that obtained using the more common model, as illustrated in Fig. 8. Figure 9 shows a comparison at large orifice openings. It is clear that the representation of the empirical model at large orifice openings is excellent.

Figure 10 shows a comparison of the empirically predicted and measured flow rates as a function of pressure drop across the orifice at the null position ($x = 0$). The tangent on the curve represents the flow pressure coefficient at operating points, $x = 0$ and $\Delta P = 6$ MPa. Figure 11 also shows a comparison of the flow rate as a function of pressure drop across the orifice at an opening of 0.5 mm.

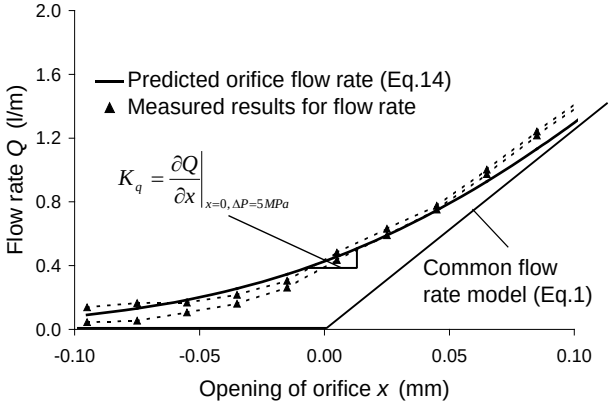

Fig. 8: *Comparison of model-based and experimental results of orifice flow rate at ΔP = 5MPa (for small openings (x > 0) and small lapped amounts (x < 0))*

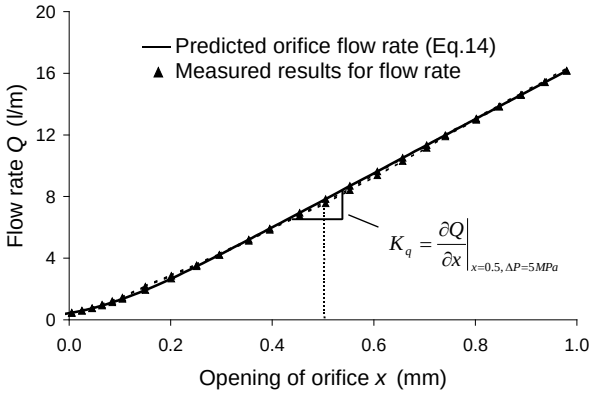

Fig. 9: *Comparison of model-based and experimental results of orifice flow rate at ΔP = 5MPa (for large openings)*

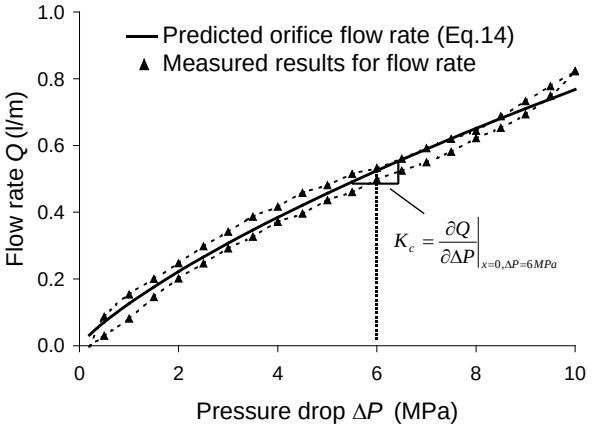

Fig. 10: *Comparison of model-based and experimental results of orifice flow rate at x = 0*

Figure 12 shows a comparison of the orifice flow gains, K_q, based on the empirical model and experimental results. The two curves plotted with "triangles" represent experimental flow gains, i.e. the slopes of the upper and lower dashed lines shown in Fig. 8 and 9. The experimental results show a flat region at about x = 0.2 mm. This is attributed to the fact that K_q (experimental) is obtained graphically and in this region, small variations can lead to large errors in the slope.

Figure 13 compares the orifice flow pressure coefficients, K_c, based on the empirical model and slope values obtained from the experimental results. The solid line represents the predicted results from the empirical model. The scatter evident in the experimental results of Fig. 13 is attributed to the process of differentiation of the experimental data, which also has a significant amount of scatter.

There is a relatively good agreement between the empirical model predictions and the experimental results. The determination of K_q and K_c using Eq. 15 and 16 is a valid approach.

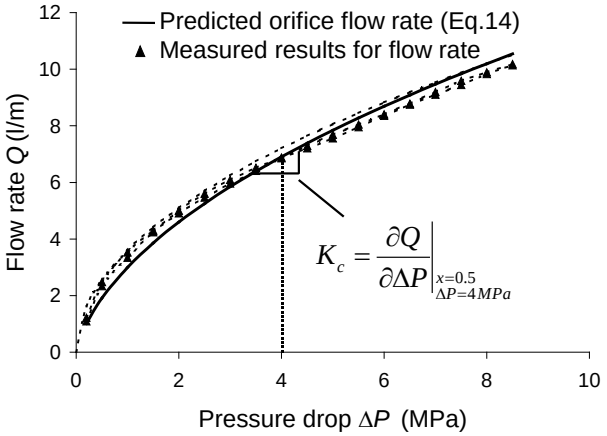

Fig. 11: *Comparison of model-based and experimental results of orifice flow rate at x = 0.5 mm*

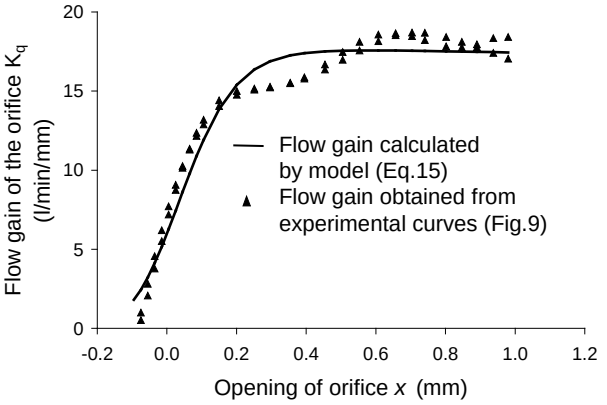

Fig. 12: *Comparison of modeled and experimental flow gain with the pressure drop of 5 MPa*

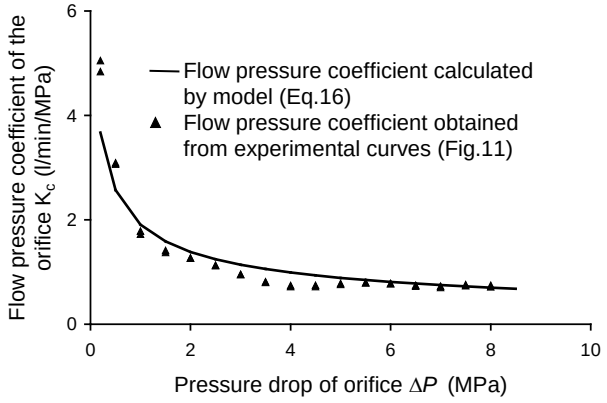

Fig. 13: *Comparison of modeled and experimental flow pressure coefficient with the orifice opening of 0.5 mm*

5 Conclusions

The flow rate through a pilot valve usually is small due to small orifice openings. A problem occurs in using the classical orifice flow equation in this case. The discharge coefficient is not a constant due to laminar flow conditions. In addition, it is difficult to determine the actual orifice cross-sectional area about the null position due to clearances, chamfers, and machining limitations. This paper provides an empirical flow cross-sectional area model that includes only one parameter, d_0, or only two parameters, d_0 and w, for non-rectangular orifice. In practice, C_d must also be measured (for example, Wu (2002), which requires measurement of other parameters). It is thus possible to differentiate the flow equations with respect to the orifice opening and pressure drop in order to obtain the flow gain and flow pressure coefficient of the pilot valve. Thus, the discontinuity problem of applying the traditional flow rate model at $x = 0$ no longer exists. A comparison between experimental and empirical models show that this approach is valid.

Nomenclature

A	orifice cross-sectional area	[m^2]
A_0	orifice cross-sectional area at the zeroed orifice opening	[m^2]
a, b	coefficients in the empirical model C_d, or polynomials	[-]
C_d	discharge coefficient	[-]
$C_{d\infty}$	turbulent discharge coefficient	[-]
d	height of square type orifice	[m]
d_0	height of square type orifice at the null position	[m]
K_q	flow gain	
K_{q0}	flow gain at the zeroed orifice opening	
K_c	flow pressure coefficient	
K_{c0}	flow pressure coefficient at the zeroed orifice opening	
N	the number of experiments	[-]
P_d	downstream pressure	[Pa]
P_u	upstream pressure	[Pa]
ΔP	pressure drop across orifice	[Pa]
Q	volumetric flow rate	[m^3/s]
Re	Reynolds number	[-]
w	rectangular orifice width	[m]
x	orifice opening	[m]
X	dimensionless orifice opening	[-]
α	a small orifice opening	
δ	laminar flow discharge coefficient	[-]
δ_1 δ_2	attenuation coefficients of the empirical model modification associated with discharge coefficient	[-]
ρ	fluid density	[kg/m^3]

Acknowledgements

The authors are grateful to visiting professor Jian Ruan from Zhejiang University of Technology of China for his helpful suggestions. This research was made possible through the financial support of NSERC grants RGPIN 17061-99 and RGPIN 3689-00.

References

Bitner, D. 1986. *Analytical and Experimental Analysis of a Load Sensing Pump*. M. Sc. thesis, University of Saskatchewan, Canada.

Chaimowitsch, E. M. 1967. *Ölhydraulik: Grundlagen und Anwendung*. Veb Verlag Technik Berlin.

Krus, P. 1988. *On Load Sensing Fluid Power Systems*. Dissertation No. 198, Linkoping University, Sweden.

Lantto, B., Palmberg, J. O. and **Krus, P.** 1990. Static and Dynamic Performance of Mobile Load-sensing Systems with Two Different Types of Pressure-Compensated Valves. *SAE Technical Paper Series*. SAE, Sept 10-13, pp. 251.

Lantto, B., Krus, P. and **Palmberg, J. O.** 1991. Interaction between Loads in Load-sensing Systems. *Proceeding of the 2nd Tampere International Conference on Fluid Power*. Linkoping, Sweden, pp. 53.

Merritt, H. E. 1967. *Hydraulic Control Systems*. John Wiley & Sons, Inc.

Palmberg, J. O., Krus, P. and **Ding, K.** 1985. Dynamic Response Characteristics of Pressure-Control Pumps. *The 1st International Conference on Fluid Power Transmission and Control*, Zhejiang University, Hangzhou, China, pp. 110.

Pettersson, H., Krus, P., Jansson, A. and **Palmberg, J. O.** 1996. The Design of Pressure Compensators for Load Sensing Hydraulic systems. *UKACC International Conference on Control'96*, IEE 427, University of Exeter, UK, pp. 1456.

Wu, D. 2002. *Analysis and Simulation of LSPC Hydraulic Systems*. Ph.D. thesis, University of Saskatchewan, work in progress.

Appendix A

Derivation of the general form of flow gain and flow pressure coefficient through orifices

For simplicity, the orifice flow equation (Eq. 2) can be re-expressed as

$$Q = C_d A \sqrt{\frac{2}{\rho}\Delta P} \tag{A1}$$

where

$$C_d = C_{d\infty}\left(1 + a \cdot e^{-\frac{\delta_1}{C_{d\infty}}\sqrt{Re}} + b \cdot e^{-\frac{\delta_2}{C_{d\infty}}\sqrt{Re}}\right) \quad \text{(A2)}$$

$$A = \frac{wx}{1 - e^{-\frac{x}{d_0}}} \quad \text{(A3)}$$

For a rectangular orifice with width w, when the orifice opening, x, is much less than width w (i.e., $x << w$), the Reynolds number can be expressed as (Wu, 2002)

$$Re = \frac{2Q\rho}{w\mu} \quad \text{(A4)}$$

Differentiating Eq. A1 with respect to orifice opening, x, gives

$$K_q = \frac{\partial Q}{\partial x} = A\sqrt{\frac{2}{\rho}\Delta P}\,\frac{\partial C_d}{\partial x} + C_d\sqrt{\frac{2}{\rho}\Delta P}\,\frac{\partial A}{\partial x} \quad \text{(A5)}$$

where

$$\frac{\partial C_d}{\partial x} = \frac{dC_d}{d\sqrt{Re}}\frac{d\sqrt{Re}}{dQ}\frac{\partial Q}{\partial x} = \left(-a\delta_1 e^{-\frac{\delta_1}{C_{d\infty}}\sqrt{Re}} - b\delta_2 e^{-\frac{\delta_2}{C_{d\infty}}\sqrt{Re}}\right)\cdot\sqrt{\frac{\rho}{2w\mu Q}}\cdot\frac{\partial Q}{\partial x} \quad \text{(A6)}$$

$$\frac{\partial A}{\partial x} = w\frac{\left(1 - (1+X)\cdot e^{-X}\right)}{\left(1 - e^{-X}\right)^2} \quad \text{(A7)}$$

X is a dimensionless number ($X = x/d_0$). Substituting Eq. A6 and A7 into Eq. A5 gives

$$\frac{\partial Q}{\partial x} = \left(-a\delta_1 e^{-\frac{\delta_1}{C_{d\infty}}\sqrt{Re}} - b\delta_2 e^{-\frac{\delta_2}{C_{d\infty}}\sqrt{Re}}\right)\cdot\sqrt{\frac{\rho}{2w\mu Q}}\cdot A\sqrt{\frac{2}{\rho}\Delta P}\,\frac{\partial Q}{\partial x} + C_d w\frac{\left(1 - (1+X)\cdot e^{-X}\right)}{\left(1 - e^{-X}\right)^2}\sqrt{\frac{2}{\rho}\Delta P}$$
$$= \frac{\left(-a\delta_1 e^{-\frac{\delta_1}{C_{d\infty}}\sqrt{Re}} - b\delta_2 e^{-\frac{\delta_2}{C_{d\infty}}\sqrt{Re}}\right)\sqrt{Re}}{2C_d}\frac{\partial Q}{\partial x} + C_d w\frac{\left(1 - (1+X)\cdot e^{-X}\right)}{\left(1 - e^{-X}\right)^2}\sqrt{\frac{2}{\rho}\Delta P} \quad \text{(A8)}$$

The first term in the right hand side can be considered as the product of a coefficient, ε, and $\partial Q/\partial x$. K_q (i.e. $\partial Q/\partial x$) is then solved to be

$$K_q = \frac{\partial Q}{\partial x} = \frac{C_d w}{1 - \varepsilon}\frac{\left(1 - (1+X)\cdot e^{-X}\right)}{\left(1 - e^{-X}\right)^2}\sqrt{\frac{2}{\rho}\Delta P} \quad \text{(A9)}$$

where

$$\varepsilon = \frac{\left(-a\delta_1 e^{-\frac{\delta_1}{C_{d\infty}}\sqrt{Re}} - b\delta_2 e^{-\frac{\delta_2}{C_{d\infty}}\sqrt{Re}}\right)\sqrt{Re}}{2C_d} \quad \text{(A10)}$$

Similarly, differentiating Eq. A1 with respect to pressure drop, ΔP, gives

$$K_c = \frac{\partial Q}{\partial \Delta P} = A\sqrt{\frac{2}{\rho}\Delta P}\,\frac{\partial C_d}{\partial \Delta P} + \frac{C_d A}{\sqrt{2\rho\Delta P}} = \varepsilon K_c + \frac{C_d A}{\sqrt{2\rho\Delta P}}$$

or

$$K_c = \frac{\partial Q}{\partial \Delta P} = \frac{C_d wx}{(1-\varepsilon)\left(1 - e^{-X}\right)\sqrt{2\rho\Delta P}} \quad \text{(A11)}$$

It is notable that when $x = 0$ (hence $X = 0$), Q, K_q and K_c show the form of 0/0. Similar to Eq. 13, the value of Q, K_q and K_c at the null position can be calculated by

$$Q_0 = C_d w d_0\sqrt{\frac{2}{\rho}\Delta P} \quad \text{(A12)}$$

$$K_{q0} = \frac{\partial Q}{\partial x} = \frac{C_d w}{2(1-\varepsilon)}\sqrt{\frac{2}{\rho}\Delta P} \quad \text{(A13)}$$

$$K_{c0} = \frac{\partial Q}{\partial \Delta P} = \frac{C_d w d_0}{(1-\varepsilon)\sqrt{2\rho\Delta P}} \quad \text{(A14)}$$

Appendix B

Derivation of the flow gain and the flow pressure coefficient for the laminar flow through orifices

Equation 2 is an empirical orifice flow equation that can be applied to both laminar and turbulent flow. Eq. 15 and 16 are the flow gain, K_q, and the flow pressure coefficient, K_c, developed from Eq. 2. When the flow through orifices becomes laminar, the Reynolds number of the orifice flow is very small and the discharge coefficient can be approximated by its linearization model, i.e.,

$$C_d = \delta\sqrt{Re} \quad \text{(B1)}$$

where $\delta = -a\cdot\delta_1 - b\cdot\delta_2$. Substituting Eq. A4 into Eq. B1 gives

$$C_d = \delta\sqrt{\frac{2Q\rho}{w\mu}} \quad \text{(B2)}$$

Replacing Eq. A2 by Eq. B2, Eq. A1 becomes

$$Q = \frac{2\delta x}{1 - e^{-\frac{x}{d_0}}}\sqrt{\frac{wQ\Delta P}{\mu}}$$

or

$$\sqrt{Q} = \frac{2\delta x}{1 - \mathrm{e}^{-\frac{x}{d_0}}} \sqrt{\frac{w\Delta P}{\mu}} \qquad \text{(B3)}$$

Squaring both sides of Eq. B3 results in the laminar flow equation of an orifice as

$$Q = \frac{4\delta^2 x^2 w\Delta P}{\mu\left(1 - \mathrm{e}^{-\frac{x}{d_0}}\right)^2} \qquad \text{(B4)}$$

Equation B4 shows a linear relationship between the orifice flow and pressure drop. Eq. B4 can be compared to Eq. (3-39) of Merritt (1967) (note: the term of $4x^2w$ is same as $2D_hA$ in Merritt). The only difference is that the term of the exponential function, $\left(1 - \mathrm{e}^{-\frac{x}{d_0}}\right)^2$ exists in the denominator of Eq. B4.

Differentiating Eq. B4 with respect to x and ΔP gives the flow gain and the flow pressure coefficient at the laminar flow condition as

$$K_a = \frac{\partial Q}{\partial x} = \frac{8\delta^2 wx\Delta P}{\mu} \cdot \frac{1 - (1 + X)\cdot \mathrm{e}^{-X}}{\left(1 - \mathrm{e}^{-X}\right)^3} \qquad \text{(B5)}$$

$$K_c = \frac{\partial Q}{\partial \Delta P} = \frac{4wx^2\delta^2}{\mu\left(1 - \mathrm{e}^{-\frac{x}{d_0}}\right)^2} \qquad \text{(B6)}$$

Duqiang Wu
Graduate student for Ph.D. at present, Mechanical Engineering Department, University of Saskatchewan in Canada. Master (1984) at Nanjing University of science and Technology in China. Engineer (1986) at Shaanxi Mechanical and Electrical Institute in China. Visiting Scholar (1997) at University of Illinois at Urbana-Champaign.

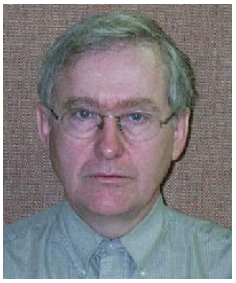

Richard Burton
P.Eng, Ph.D, Assistant Dean of the college of Engineering, Professor, Mechanical Engineering, University of Saskatchewan. Burton is involved in research pertaining to the application of intelligent theories to control and monitoring of hydraulics systems, component design, and system analysis. He is a member of the executive of ASME, FPST Division, a member of the hydraulics' advisory board of SAE and NCFP and a convenor for FPNI.

Greg Schoenau
Professor of Mechanical Engineering at the University of Saskatchewan. He was head of that Department from 1993 to 1999. He obtained B.Sc. and M. Sc. Degrees from the University of Saskatchewan in mechanical engineering in 1967 and 1969, respectively. In 1974 he obtained his Ph.D. from the University of New Hampshire in fluid power control systems. He continues to be active in research in this area and in the thermal systems area as well. He has also held positions in numerous outside engineering and technical organizations.

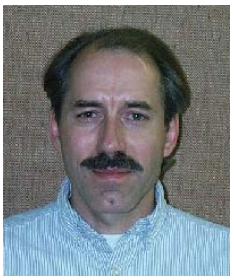

Doug Bitner
MSc. Departmental Assistant Mechanical Engineering, University of Saskatchewan. Manager Fluid Power Laboratory and Control Systems Laboratory University of Saskatchewan.